NANO LETTERS

Letter

pubs.acs.org/NanoLett

Direct Observation of Heterogeneous Amyloid Fibril Growth Kinetics via Two-Color Super-Resolution Microscopy

Dorothea Pinotsi,*[,†] Alexander K. Buell,[‡] Celine Galvagnion,[‡] Christopher M. Dobson,[‡] Gabriele S. Kaminski Schierle,*[,†] and Clemens F. Kaminski*[,†]

[†]Department of Chemical Engineering and Biotechnology and [‡]Department of Chemistry, University of Cambridge, Cambridge, United Kingdom

Supporting Information

ABSTRACT: The self-assembly of normally soluble proteins into fibrillar amyloid structures is associated with a range of neurodegenerative disorders, such as Parkinson's and Alzheimer's diseases. In the present study, we show that specific events in the kinetics of the complex, multistep aggregation process of one such protein, α-synuclein, whose aggregation is a characteristic hallmark of Parkinson's disease, can be followed at the molecular level using optical super-resolution microscopy. We have explored in particular the elongation of preformed α-synuclein fibrils; using two-color single-molecule localization microscopy we are able to provide conclusive evidence that the elongation proceeds from both ends of the fibril seeds. Furthermore, the technique reveals a large heterogeneity in the growth rates of individual fibrils; some fibrils exhibit no detectable growth, whereas others extend to more than ten times their original length within hours. These large variations in the growth kinetics can be attributed to fibril structural polymorphism. Our technique offers new capabilities in the study of amyloid growth dynamics at the molecular level and is readily translated to the study of the self-assembly of other nanostructures.

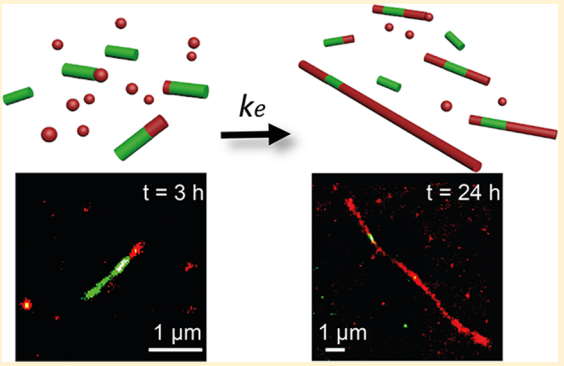

KEYWORDS: *Two-color super-resolution microscopy, aggregation kinetics, amyloid fibril self-assembly, α-synuclein, fibril polymorphism*

The phenomenon of the self-assembly of functional proteins into amyloid fibrils and its relationship to medical conditions such as Parkinson's and Alzheimer's diseases have been the focus of intense research efforts in recent years.[1,2] Considerable insight has been gained from both experimental and theoretical studies into the events that contribute to the overall conversion of soluble proteins to their aggregated states, although much remains to be ascertained about the individual molecular steps involved in such processes.[3−5] Of particular importance in this context is the ability to probe at high resolution the various structural mechanisms involved in the initiation and growth of different fibrillar states. Fibril growth kinetics are most commonly studied *in vitro*, using assays based on the enhancement of fluorescence of dyes, such as Thioflavin-T (ThT) or by using surface-based biosensing assays,[4] both of which measure the growth of large numbers of aggregates. Such measurements are valuable for determining average rate constants via kinetic models and global data fitting,[5] although it is becoming increasingly clear that the underlying processes depend significantly on factors such as size, nature and local environment of individual aggregate species.

Studies in which individual aggregates can be visualized using techniques such as TIRF-ThT (total internal reflection-Thioflavin-T)[6−9] and *in situ* atomic force microscopy (AFM)[10−15] shed new light into the complex nature of the individual molecular steps involved in the kinetics of aggregation reactions, including the way in which fibrils can elongate by addition of further soluble molecular species, providing information that is not available from ensemble measurements. Several of these studies have postulated that amyloid fibrils grow via a "stop-and-go" mechanism,[6,8,13,14,16] that is, that at any given time only a fraction of all fibrils undergo elongation. One issue of considerable interest is the extent to which individual fibrils have similar growth statistics, and whether or not there are distinct populations exhibiting variable growth rates over an extended period of time. This question is of particular relevance in the context of the existence and propagation of different morphologically defined species leading to distinct pathological phenotypes, a mechanism often referred to as templating.[17]

In this paper, we use super-resolution microscopy[18−23] to visualize directly the growth of individual amyloid fibrils. This technique has recently been applied in studies of amyloid morphology both in aqueous solution[24,25] and in cells.[26−28] In the present study we use two-color *direct* Stochastic Optical

Received: November 5, 2013
Revised: November 26, 2013

   dx.doi.org/10.1021/nl4041093 | *Nano Lett.* XXXX, XXX, XXX−XXX

Reconstruction Microscopy (*d*STORM) as a powerful means of elucidating the nature and the kinetics of the growth of individual fibrils *in vitro*, through its ability to distinguish by color those regions of fibrils formed at different stages of the reaction, providing details on the molecular level of the process. Using differently labeled fibrillar seeds and monomers of α-synuclein, a protein involved in Parkinson's disease, we are able to distinguish clearly individual fibrils formed at different stages of the aggregation reaction as a result of the high spatial resolution of better than 20 nm. Furthermore, we provide clear evidence that fibril growth is bidirectional, a subject of considerable debate in the amyloid field.[6,7,9,10,12,13,27] In addition, we establish that elongation is a highly heterogeneous process, which cannot be fully described by a single rate constant. We discuss possible molecular origins for the observed variations in the growth kinetics and speculate that these variations could be significant in the context of onset and propagation of disease.

Amyloid Growth from Seed Fibrils Is a Bidirectional Process. In order to visualize α-synuclein fibrils using *d*STORM, we prepared separate batches of covalently labeled cysteine variants (N122C) of the protein with Alexa Fluor 647 (AF647) and with Alexa Fluor 568 (AF568) dyes (Invitrogen, Carlsbad, CA, U.S.A.) (see Materials and Methods in Supporting Information). We verified that the dye labels do not interfere with the aggregation process and that the fibril morphology and the kinetics of fibril formation are indistinguishable from those of the unlabeled protein, as revealed by AFM and ThT assays (see Supporting Information). We chose to use direct covalent labeling of α-synuclein rather than immunofluorescence staining because of the very small size of the Alexa dye labels compared to antibody molecules, and because of the high specificity of labeling afforded by use of covalent linkages, both of which result in an increase in the resolution of the imaging process.[25,26] We found the optimal labeling ratio for two-color *d*STORM to be ca. 1:20 for the fraction of labeled relative to unlabeled protein; too high a labeling density would compromise resolution (by increasing the likelihood that proximate fluorophores emit simultaneously and therefore cause mislocalization) and might potentially lead to steric interferences of the dye with the amyloid protein. Figure 1a,c show the conventional, diffraction limited fluorescence images of α-synuclein fibrils; the corresponding *d*STORM images are shown in Figure 1b,d. From the *d*STORM images, we inferred an average fibril diameter of 18 ± 2 nm, which shows that the resolution achieved approaches that of techniques such as AFM.[29]

Having established that α-synuclein fibrils can be reliably imaged using our super-resolution technique, we proceeded to perform two-color *d*STORM experiments and to analyze the dynamics of fibril growth. We visualized the process of fibril elongation using a seeded aggregation assay;[30,31] the starting point was a solution of preformed fibrils of α-synuclein with an average length of 400 nm, labeled at 5% with AF568 (green) (see Materials and Methods in Supporting Information for details). At the start of each such assay, a solution containing α-synuclein in its monomeric state with 5% of the protein molecules labeled with AF647 (red) was added to the initial sample at a 10-fold excess (by mass); under these conditions the only relevant molecular process is elongation,[31,32] permitting the direct measurement of the rates of this specific process. The solution was left to incubate for 24 h at 37 °C and under quiescent conditions in which breakage of fibrils is minimal. At different time points during the aggregation reaction aliquots were taken from the solution and deposited onto glass coverslip chambers containing photoswitching buffer, optimized for two-color *d*STORM (see Materials and Methods in Supporting Information). The fibrils had therefore been allowed to elongate in bulk solution in the absence of any sample-substrate interactions that might have affected the growth kinetics.[11,13] Figure 2 shows the elongation of the seed fibrils as a function of time. In Figure 2a, the seed fibrils, labeled with green AF568, are shown before addition of the monomeric protein. At the beginning of the experiment (t = 0 h) monomeric protein labeled with red AF647 was added and two-color super-resolution images were recorded at different time points during 24 h of fibril growth, as shown in Figure 2b–h.

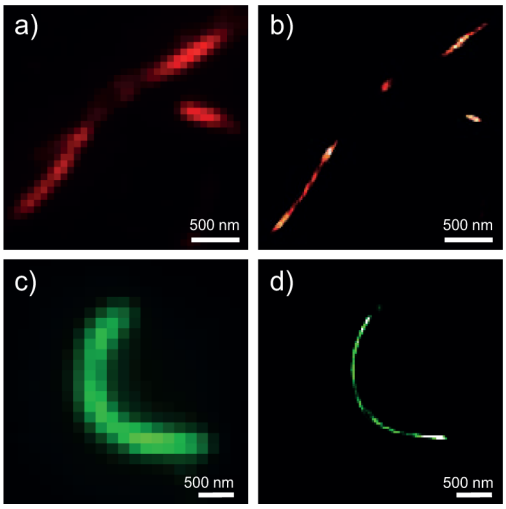

Figure 1. Comparison of conventional fluorescence and super-resolution images of directly labeled amyloid fibrils of α-synuclein: (a,c) conventional (diffraction limited) fluorescence images of the fibrils, labeled with AF647 and AF568, respectively; (b,d) corresponding *d*STORM images, demonstrating the dramatic resolution enhancement obtainable over conventional imaging.

Using two-color *d*STORM we are able to distinguish between the seed fibrils initially present (indicated by arrowheads and rendered in green color) and the freshly added protein (indicated by arrows and rendered in red color). We can therefore monitor the process of fibril elongation over hours or even days in the absence of any destructive sample preparation steps such as drying or shaking, which are known to induce breakage. Indeed, fibril breakage was observed to be negligible in our experiments, as all fibrils we had imaged contained either elements of both green fluorescence (AF568 from the seed species) and red fluorescence (AF647, signifying the newly added protein), or just green fluorescence (AF568, the latter also indicating that no detectable growth had taken place); no fibrils were observed that were solely labeled with red fluorophores, indicating that neither monomer nucleation, nor fibril breakage were significant under the experimental conditions reported here. In contrast to conventional TIRF fluorescence imaging (Figure 2i), two-color *d*STORM (Figure 2h) clearly distinguishes between the original fibril seeds and the grown regions of the fibrils. Importantly, our data establish unambiguously that α-synuclein fibril elongation under the conditions used here is a bidirectional process, that is, that it proceeds from both ends of fibril seeds. In previous experiments, both bidirectional[10,12,13] and unidirectional[6,7,9]

dx.doi.org/10.1021/nl4041093 | *Nano Lett.* XXXX, XXX, XXX–XXX

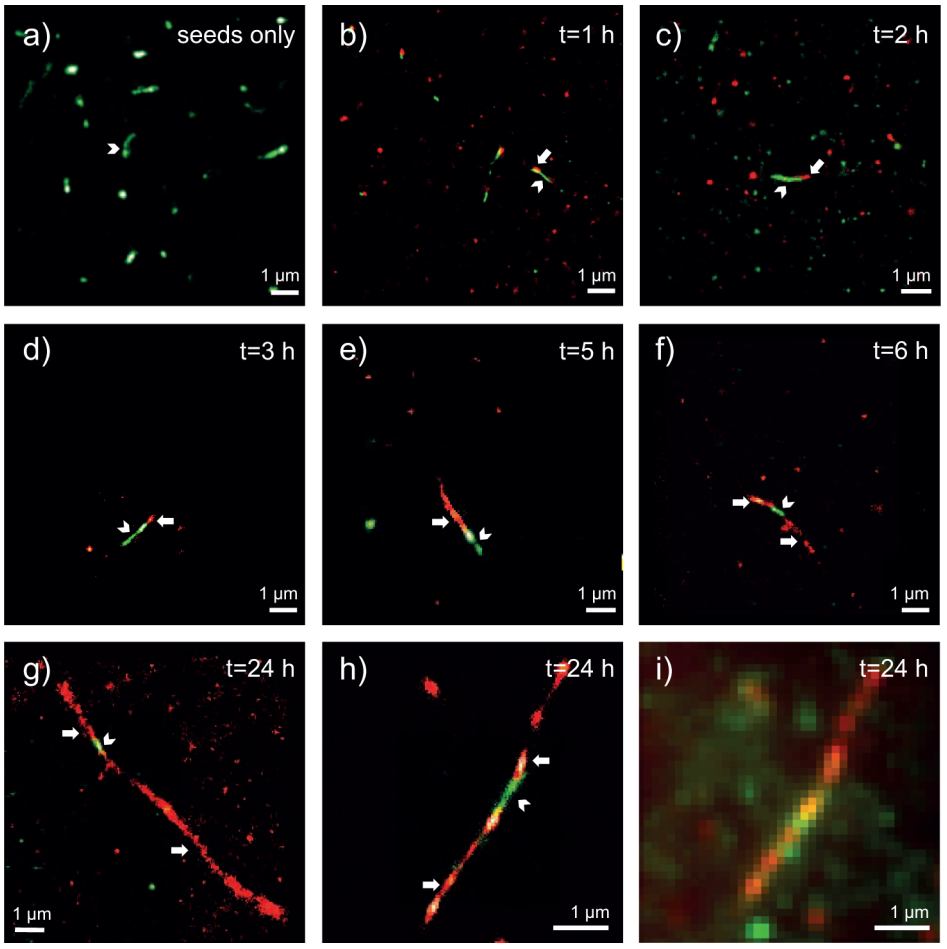

Figure 2. Two-color *d*STORM images reveal details of the elongation of α-synuclein fibrils through addition of soluble protein molecules, *in vitro*. (a) The initial sample consists of α-synuclein seed fibrils at 8 μM concentration, labeled with AF568 (green). At $t = 0$ h, monomeric α-synuclein at a total concentration of 80 μM (76 μM wild type, 4 μM AF647-labeled N122C) (red) was added to the solution. (b–h) Aliquots were taken during the aggregation reaction and imaged with two-color *d*STORM. The images show the overlay of the two channels (green, AF568 and red, AF647). The time points after the initiation of aggregation are (b) $t = 1$ h, (c) $t = 2$ h, (d) $t = 3$ h, (e) $t = 5$ h, (f) $t = 6$ h, and (g,h) $t = 24$ h. Each fibril consists of the initial seed (green, indicated by an arrowhead) and the extended region formed through addition of monomeric protein (red, indicated by an arrow). The lengths of the fibrils reach several micrometers with the initial seed fibril being extended from both ends. (h) Two-color *d*STORM image of a fibril at $t = 24$ h and (i) conventional fluorescence image in TIRF of the same fibril as in (h), showing that the increase in resolution achieved by *d*STORM enables the original and the newly formed section of the fibril to be clearly distinguished.

growth of different amyloid fibrils such as Aβ, amylin, and α-synuclein have been reported, although issues such as substrate interference with fibril growth could not be excluded, or the resolution from conventional techniques was limited. Here, the elongation reaction occurs in an undisturbed environment in bulk solution, and hence is unaffected by such interference. Furthermore, the resolution achieved with two-color *d*STORM enables to conclusively establish that fibril growth is bidirectional.

We performed additional control experiments using solutions containing either seed fibrils in the absence of monomeric protein, or solutions containing monomeric protein in the absence of seed fibrils. Incubation of these samples for 24 h at 37 °C resulted in no observable fibril elongation or fibril formation (see Supporting Information Figure 3). These results confirm that seed fibrils are inert in the absence of monomeric protein and therefore do not, for example, join together by mutual interaction of their free ends. Also, *de novo* formation of α-synuclein amyloid fibrils via primary nucleation occurs at a negligible rate relative to fibril growth, confirming elongation of seeds as the only significant process during the aggregation reactions presented here.

Analysis of Fibril Elongation Kinetics Reveals Inhomogeneous Growth Rates and Distinct Fibril Populations. In order to investigate possible variations in growth kinetics for individual fibrils, we analyzed multiple *d*STORM images of growing fibrils, recorded at different time points during the aggregation reaction and in different regions of the glass coverslips (see Materials and Methods in Supporting Information for details); we then studied the distribution of elongation values as a function of time. In Figure 3a, histograms of the measured elongation lengths of individual fibrils are shown (*d*STORM, red channel) for different time points up to 24 h of the aggregation reaction. The width of the observed distributions of fibril elongation values can be seen to increase significantly with time; for example, after $t = 24$ h, some fibrils have reached lengths of up to 7 μm, but others show either no, or only a very small, increase in length. In Figure 3b, we have plotted the histograms of the corresponding average growth "velocities" (calculated as the length increase divided by the overall growth time) at the same time points as depicted in

dx.doi.org/10.1021/nl4041093 | *Nano Lett.* XXXX, XXX, XXX–XXX

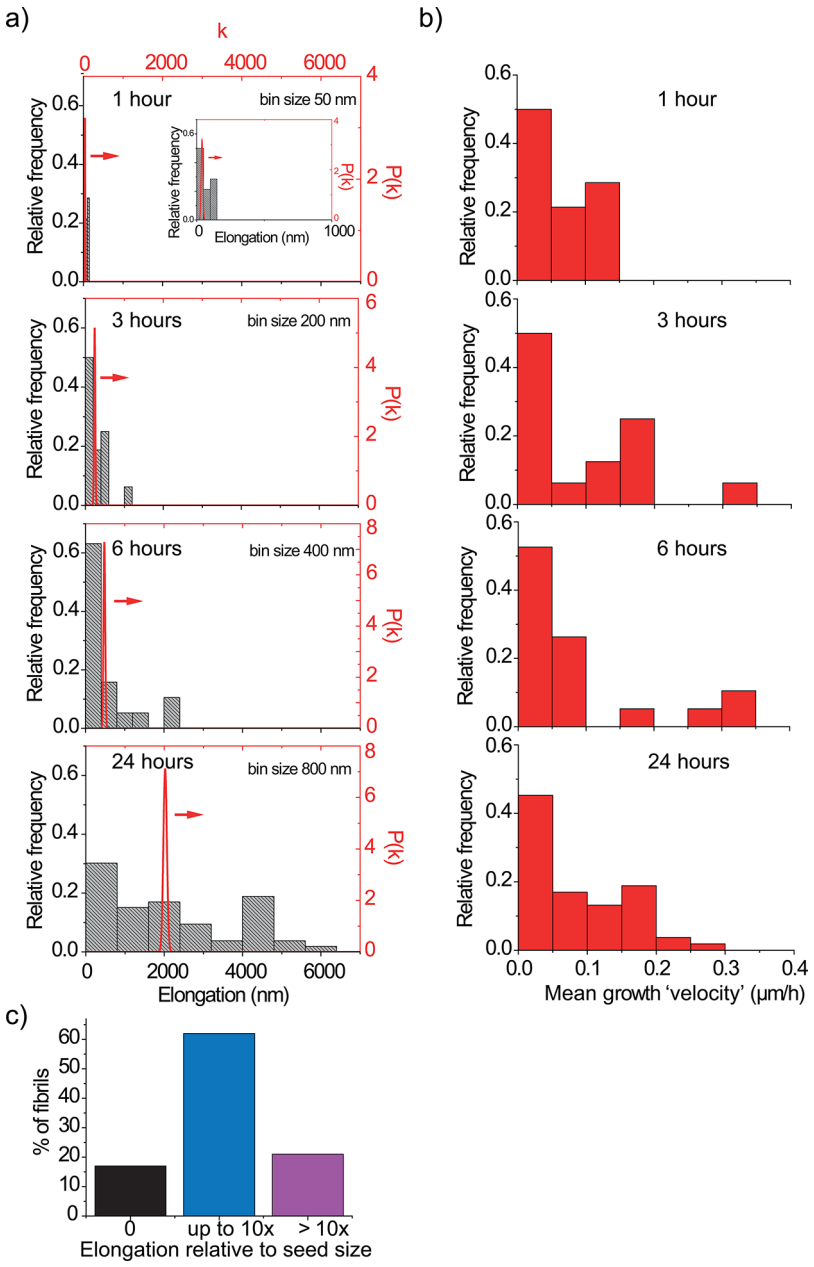

Figure 3. Histograms of the distributions of elongation lengths (corresponding to the newly formed (red) regions) of seed fibrils. The histograms in panel (a) show the relative frequency of different elongation lengths obtained at 1, 3, 6, and 24 h. A curve depicting the Poisson distribution for the number of attached monomers with the same average value as the average elongation value obtained from the histogram is overlaid at each time point. The *x*-axis label, *k*, corresponds to the number of attached monomers divided by 2, assuming that each monomer has a length of 0.5 nm. (b) Histograms showing the relative frequency of the mean growth "velocities" over the same time points as in (a). The bin size is 0.05 μm/h. (c) Diagram summarizing the distribution of the elongation values of fibrils at the end of the incubation process (t = 24 h). Black bar: percentage of fibrils that exhibit zero growth (no detectable red regions). Blue bar: percentage of fibrils that have grown to a size ranging from the lowest detectable length to up to 10 times the length of the initial seed. Violet bar: percentage of fibrils that have elongated by more than 10 times the length of the initial seed fibril.

Figure 3a. These histograms show that the variation in elongation rates remains approximately constant over time, indicating that at each time point there is a range of fibrils displaying distinct growth rates.

We further investigated the two extreme elongation values; namely the frequency of the occurrence of seeds that show no detectable growth (denoted by the absence of any red regions that would indicate that fibril elongation had taken place) or that of species exhibiting very fast growth rates. The most striking feature of the data presented in Figure 3c is that a significant proportion of seed fibrils (17%) did not exhibit any growth in the presence of monomeric protein and remained at their initial length.[33] In contrast, the majority of the fibrils (63%) grew up to 10 times their initial length in 24 h; indeed, a small fraction of fibrils (20%) grew more than 10 times their initial length. Taking the average of all individual rates observed, including data from fibrils that had not elongated, we obtained a mean growth rate of 1.4 nm/min over 24 h, with a standard deviation of 1 nm/min, which is in good agreement with the values for average growth rates obtained using ThT

dx.doi.org/10.1021/nl4041093 | *Nano Lett.* XXXX, XXX, XXX−XXX

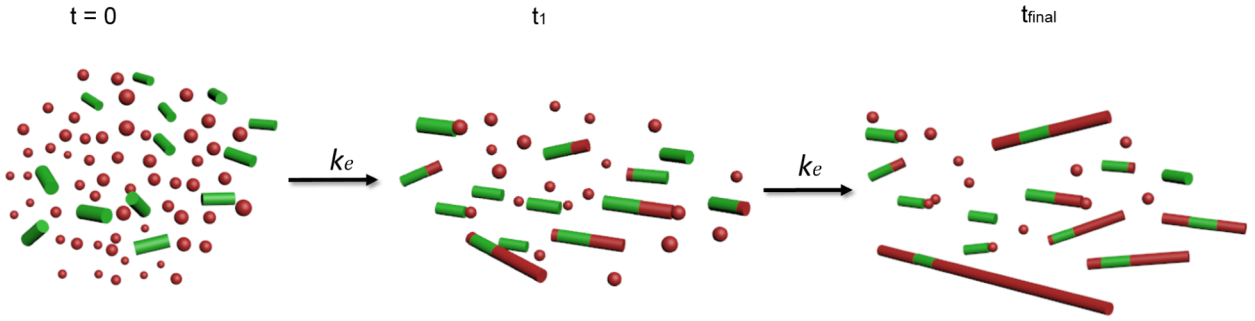

Figure 4. Schematic diagram of the elongation of α-synuclein seed fibrils, depicting the different mechanisms that influence fibril growth. The green cylinders correspond to fibrillar seeds labeled with Alexa Fluor 568 and the red spheres correspond to the monomeric protein labeled with Alexa Fluor 647. k_e denotes the average elongation rate constant.

ensemble measurements.[31] Clearly, the observed ensemble kinetics are a consequence of a larger number of elementary reaction steps that cannot be resolved in ensemble measurements in which it is assumed that the growth of all fibrils contributes equally to the observed total increase in fibril mass. Of particular interest is the finding that some seed fibrils remain inactive throughout the entire duration of the experiment (24 h) that suggests that individual seeds can have very different elongation capacities.

The Mechanism of α-Synuclein Fibril Elongation Deviates from a Purely Stochastic Process Involving Random Growth. To gain insights into possible molecular mechanisms underlying the observed variations in elongation rates we carried out a more detailed analysis of rate distributions and studied the results in the context of different models of fibril elongation. For a random (stochastic) process involving discrete events, such as the addition of monomeric protein molecules to fibril ends, the probability of a certain number of these events occurring in a given time is governed by Poisson statistics. In each histogram of Figure 3a, we have therefore overlaid curves depicting the corresponding Poisson distributions for the number of attached monomers, based on the averages of the elongation values obtained from the histograms and assuming that addition of a single monomer of α-synuclein leads to a fibril length increase of 0.5 nm.[31] The data indicate that the measured distributions are not at all represented by Poisson distributions and that much larger variations in elongation rates are observed than predicted by this analysis, again indicating rapid growth of certain fibrils whereas others exhibit imperceptible growth, as schematically depicted in Figure 4.

A different model to account for inhomogenous growth kinetics invokes the so-called "stop-and-go" mechanism, which has been discussed for amyloid fibrils of $A\beta_{25-35}$[14] and glucagon.[16] In these studies, it was proposed that the origin of the observed switching between active ("go") and inactive ("stop") states lies in the occasional incorrect addition of a monomer onto a fibril end, such that the templating effect is lost until this monomer detaches or rearranges into the correctly folded state.[34] The consistency of this hypothesis with the reported in these studies data can, however, be probed by a simple argument; the free energy barrier for the dissociation of a correctly incorporated monomer from a fibril end must represent an upper bound for the energy barrier of dissociation, or for the rearrangement of improperly attached monomers, given that the correctly incorporated monomer is likely to represent the minimum in the free energy landscape.[35] The data presented in ref 14 allowed the elongation rate constants during the growth phases, k_+, to be determined as $\sim 10^6$ M^{-1} s^{-1} and the critical concentration, c_{crit} to be ~ 10 μM. At equilibrium, the fluxes of growth and dissociation are equal, and therefore the equilibrium constant is $K = 1/c_{crit} = k_+/k_{off}$, where k_{off} is the rate constant of dissociation. From this analysis we estimate $k_{off} \approx 10$ s^{-1}, which represents a rate more than 2 orders of magnitude faster than that of switching between the growth-incompetent and the growth-competent states reported in ref 14 (~ 0.03 s^{-1}). It therefore seems likely that additional factors determine the duration of the inactive periods in the experiments reported; one possibility is interactions with the surfaces on which the fibrils grow. In the present study, the seed fibrils grow in solution and are only deposited onto a surface for imaging, therefore minimizing such additional interactions.

We next explored whether or not the heterogeneous growth kinetics for individual fibrils observed in our experiments are compatible with a "stop-and-go" model. Looking at the histograms in Figure 3 it is apparent that some fibrils have inactive periods of several hours. Assuming that a fibril will become active again when an incorrectly folded monomer becomes detached at its end we can estimate using similar arguments as above whether this time scale is compatible with such a hypothesis: using a critical concentration of α-synuclein of ~ 2 μM,[35] and the determined average growth rate of $k_+ \approx 10^3 \pm 375$ M^{-1} s^{-1} (this work and ref 31) we obtain an estimate for the lower bound for the average dissociation rate, $k_{off} \approx (2.0 \pm 0.8) \times 10^{-3}$ s^{-1}. Although this value may deviate from that for individual fibrils, it cannot account for the observation that some fibrils are inactive for the entire duration of the experiment, that is, for at least 24 h. Additionally, since this process should affect fibrils of all lengths equally, it is unlikely to provide an explanation of the observed heterogeneity in fibril elongation rates. Therefore we suggest the following alternative explanations:

(1) Certain amyloid templates/seeds are not efficient in recruiting monomeric protein, leading to different fibril morphologies and growth rates (fibril polymorphism).[36] This mechanism has been proposed for several proteins such as the yeast prion Sup35,[37−39] glucagon,[40] Aβ,[41−45] tau,[46] and α-synuclein.[47,48]

(2) The spatial arrangement of fibrils, for example, because of assembly into higher order structures[31] or variations in protofilament organization,[42] may block the access needed for monomers to attach to fibril ends. Additionally, the ends of seed fibrils may become damaged during production, although this is unlikely here, because neither sample drying nor harsh fragmentation methods, such as sonication, were used.

dx.doi.org/10.1021/nl4041093 | Nano Lett. XXXX, XXX, XXX−XXX

In conclusion, we have demonstrated the development and application of two-color *d*STORM as a powerful tool for the visualization of α-synuclein fibril growth from seed templates and have carried out a quantitative analysis of the kinetics of this process. With this technique, we are able to distinguish *de novo* growth of fibrils from the original seed and to follow elongation at nanometer resolution. Our method proves conclusively that α-synuclein fibril elongation, under the conditions used here, is a bidirectional process. In addition, no end-to-end association of seed fibrils was observed to occur and elongation of seeds was evident only in the presence of monomeric protein. The kinetics of fibril growth are not adequately described by a single elongation rate parameter; rather, a large variation in growth rates was found to exist. The observed process is neither consistent with a "stop-and-go" type mechanism in which misfolded species at the fibril end need to be removed before growth can resume, nor with the notion that monomer addition is a diffusion controlled, stochastic process, for which variations in growth rates would be much smaller. We therefore suggest two alternative mechanisms that can be explored in future studies. Furthermore, the methodology described here can be readily extended to *in situ* applications in biological samples, for example, to monitor aggregation within cells and to elucidate the various parameters that affect fibril growth. It could also be used to identify different fibril strains, which may arise *in vivo*, and to investigate their role in the production and spreading of amyloidogenic species in disease.

■ ASSOCIATED CONTENT

Supporting Information

Materials and Methods section and supplementary figures. This material is available free of charge via the Internet at http://pubs.acs.org.

■ AUTHOR INFORMATION

Corresponding Authors

*E-mail: (D.P.) dp454@cam.ac.uk.
*E-mail: (G.S.K.S.) gsk20@cam.ac.uk.
*E-mail: (C.F.K.) cfk23@cam.ac.uk.

Notes

The authors declare no competing financial interest.

■ ACKNOWLEDGMENTS

This work was supported by the Medical Research Council U.K. (MR/K015850/1 and MR/K02292X/1), Alzheimer Research U.K. (ARUK-EG2012A-1), the U.K. EPSRC (EP/H018301/1), and the Wellcome Trust (089703/Z/09/Z). D.P. wishes to acknowledge support from the Swiss National Science Foundation and the Cambridge Wellcome Trust for support through personal fellowships. A.K.B. thanks Magdalene College, Cambridge, and the Leverhulme Trust for support through research fellowships.

■ REFERENCES

(1) Chiti, F.; Dobson, C. M. *Annu. Rev. Biochem.* **2006**, *75*, 333−66.
(2) Uversky, V. N. *Curr. Protein Pept. Sci.* **2008**, *9*, 507−40.
(3) Xue, W.-F.; Homans, S. W.; Radford, S. E. *Proc. Nat. Acad. Sci. U.S.A.* **2008**, *105*, 8926−8931.
(4) Knowles, T. P. J.; Shu, W.; Devlin, G. L.; Meehan, S.; Auer, S.; Dobson, C. M.; Welland, M. E. *Proc. Nat. Acad. Sci. U.S.A.* **2007**, *104*, 10016−21.
(5) Cohen, S. I. A.; Linse, S.; Luheshi, L. M.; Hellstrand, E.; White, D. A.; Rajah, L.; Otzen, D. E.; Vendruscolo, M.; Dobson, C. M.; Knowles, T. P. J. *Proc. Nat. Acad. Sci. U.S.A.* **2013**, *110*, 9758−9763.
(6) Ban, T.; Hoshino, M.; Takahashi, S.; Hamada, D.; Hasegawa, K.; Naiki, H.; Goto, Y. *J. Mol. Biol.* **2004**, *344*, 757−67.
(7) Ban, T.; Yamaguchi, K.; Goto, Y. *Acc. Chem. Res.* **2006**, *39*, 663−70.
(8) Andersen, C. B.; Yagi, H.; Manno, M.; Martorana, V.; Ban, T.; Christiansen, G.; Otzen, D. E.; Goto, Y.; Rischel, C. *Biophys. J.* **2009**, *96*, 1529−36.
(9) Patil, S. M.; Mehta, A.; Jha, S.; Alexandrescu, A. T. *Biochemistry* **2011**, *50*, 2808−19.
(10) Goldsbury, C.; Kistler, J.; Aebi, U.; Arvinte, T.; Cooper, G. J. *J. Mol. Biol.* **1999**, *285*, 33−9.
(11) Kowalewski, T.; Holtzman, D. M. *Proc. Nat. Acad. Sci. U.S.A.* **1999**, *96*, 3688−93.
(12) Blackley, H. K.; Sanders, G. H.; Davies, M. C.; Roberts, C. J.; Tendler, S. J.; Wilkinson, M. *J. J. Mol. Biol.* **2000**, *298*, 833−40.
(13) Hoyer, W.; Cherny, D.; Subramaniam, V.; Jovin, T. M. *J. Mol. Biol.* **2004**, *340*, 127−39.
(14) Kellermayer, M. S. Z.; Karsai, A.; Benke, M.; Soós, K.; Penke, B. *Proc. Nat. Acad. Sci. U.S.A.* **2008**, *105*, 141−4.
(15) Milhiet, P.-E.; Yamamoto, D.; Berthoumieu, O.; Dosset, P.; Le Grimellec, C.; Verdier, J.-M.; Marchal, S.; Ando, T. *PLoS One* **2010**, *5*, e13240.
(16) Ferkinghoff-Borg, J.; Fonslet, J.; Andersen, C. B.; Krishna, S.; Pigolotti, S.; Yagi, H.; Goto, Y.; Otzen, D.; Jensen, M. H. *Phys. Rev. E* **2010**, *82*, 010901.
(17) Prusiner, S. B.; Scott, M. R.; DeArmond, S. J.; Cohen, F. E. *Cell* **1998**, *93*, 337−48.
(18) Hell, S. W.; Wichmann, J. *Opt. Lett.* **1994**, *19*, 780.
(19) Rust, M. J.; Bates, M.; Zhuang, X. *Nat. Methods* **2006**, *3*, 793−5.
(20) Hess, S. T.; Girirajan, T. P. K.; Mason, M. D. *Biophys. J.* **2006**, *91*, 4258−72.
(21) Betzig, E.; Patterson, G. H.; Sougrat, R.; Lindwasser, O. W.; Olenych, S.; Bonifacino, J. S.; Davidson, M. W.; Lippincott-Schwartz, J.; Hess, H. F. *Science* **2006**, *313*, 1642−5.
(22) Heilemann, M.; van de Linde, S.; Schüttpelz, M.; Kasper, R.; Seefeldt, B.; Mukherjee, A.; Tinnefeld, P.; Sauer, M. *Angew. Chem., Int. Ed.* **2008**, *47*, 6172−6.
(23) Huang, B.; Wang, W.; Bates, M.; Zhuang, X. *Science* **2008**, *319*, 810−3.
(24) Duim, W. C.; Chen, B.; Frydman, J.; Moerner, W. E. *ChemPhysChem* **2011**, *12*, 2387−2390.
(25) Ries, J.; Udayar, V.; Soragni, A.; Hornemann, S.; Nilsson, K. P. R.; Riek, R.; Hock, C.; Ewers, H.; Aguzzi, A. a.; Rajendran, L. *ACS Chem. Neurosci.* **2013**, *4* (7), 1057−1061.
(26) Kaminski Schierle, G. S.; van de Linde, S.; Erdelyi, M.; Esbjörner, E. K.; Klein, T.; Rees, E.; Bertoncini, C. W.; Dobson, C. M.; Sauer, M.; Kaminski, C. F. *J. Am. Chem. Soc.* **2011**, *133*, 12902−5.
(27) Roberti, M. J.; Fölling, J.; Celej, M. S.; Bossi, M.; Jovin, T. M.; Jares-Erijman, E. A. *Biophys. J.* **2012**, *102*, 1598−607.
(28) Pinotsi, D.; Kaminski Schierle, G. S.; Rees, E.; Kaminski, C. F. *Proc. SPIE NanoSci. Eng.* **2013**, *8815*, 88150G−13.
(29) Sweers, K. K. M.; van der Werf, K. O.; Bennink, M. L.; Subramaniam, V. *ACS Nano* **2012**, *6*, 5952−60.
(30) Pinotsi, D.; Buell, A. K.; Dobson, C. M.; Kaminski Schierle, G. S.; Kaminski, C. F. *ChemBioChem* **2013**, *14*, 846−50.
(31) Buell, A.; Galvagnion, C.; Vendruscolo, M.; Knowles, T. P. J.; Dobson, C. M. Unpublished work, 2013,
(32) Cohen, S. I. A.; Vendruscolo, M.; Dobson, C. M.; Knowles, T. P. *J. Int. J. Mol. Sci.* **2011**, *12*, 5844−52.
(33) Since the protein labeling ratio was 1:20, it is possible that there is a small number of unlabeled monomeric protein molecules attached to the fibril ends which we would not have been able to detect.
(34) Esler, W. P.; Stimson, E. R.; Jennings, J. M.; Vinters, H. V.; Ghilardi, J. R.; Lee, J. P.; Mantyh, P. W.; Maggio, J. E. *Biochemistry* **2000**, *39*, 6288−6295.

(35) Baldwin, A. J.; Knowles, T. P. J.; Tartaglia, G. G.; Fitzpatrick, A. W.; Devlin, G. L.; Shammas, S. L.; Waudby, C. A.; Mossuto, M. F.; Meehan, S.; Gras, S. L.; Christodoulou, J.; Anthony-Cahill, S. J.; Barker, P. D.; Vendruscolo, M.; Dobson, C. M. *J. Am. Chem. Soc.* **2011**, *133*, 14160−14163.
(36) Eisenberg, D.; Jucker, M. *Cell* **2012**, *148*, 1188−203.
(37) DePace, A. H.; Weissman, J. S. *Nat. Struct. Biol.* **2002**, *9*, 389−96.
(38) Tanaka, M.; Chien, P.; Naber, N.; Cooke, R.; Weissman, J. S. *Nature* **2004**, *428*, 323−328.
(39) Toyama, B. H.; Kelly, M. J. S.; Gross, J. D.; Weissman, J. S. *Nature* **2007**, *449*, 233−7.
(40) Pedersen, J. S. n.; Dikov, D.; Flink, J. L.; Hjuler, H. A.; Christiansen, G.; Otzen, D. E. *J. Mol. Biol.* **2006**, *355*, 501−23.
(41) Petkova, A. T.; Leapman, R. D.; Guo, Z.; Yau, W.-M.; Mattson, M. P.; Tycko, R. *Science* **2005**, *307*, 262−5.
(42) Meinhardt, J.; Sachse, C.; Hortschansky, P.; Grigorieff, N.; Fändrich, M. *J. Mol. Biol.* **2009**, *386*, 869−77.
(43) Kodali, R.; Williams, A. D.; Chemuru, S.; Wetzel, R. *J. Mol. Biol.* **2010**, *401*, 503−17.
(44) Qiang, W.; Kelley, K.; Tycko, R. *J. Am. Chem. Soc.* **2013**, *135*, 6860−71.
(45) Ban, T.; Hamada, D.; Hasegawa, K.; Naiki, H.; Goto, Y. *J. Biol. Chem.* **2003**, *278*, 16462−5.
(46) Furukawa, Y.; Kaneko, K.; Nukina, N. *J. Biol. Chem.* **2011**, *286*, 27236−46.
(47) Guo, J. L.; Covell, D. J.; Daniels, J. P.; Iba, M.; Stieber, A.; Zhang, B.; Riddle, D. M.; Kwong, L. K.; Xu, Y.; Trojanowski, J. Q.; Lee, V. M. Y. *Cell* **2013**, *154*, 103−17.
(48) Bousset, L.; Pieri, L.; Ruiz-Arlandis, G.; Gath, J.; Jensen, P. H.; Habenstein, B.; Madiona, K.; Olieric, V.; Böckmann, A.; Meier, B. H.; Melki, R. *Nat. Commun.* **2013**, *4*, 2575.

dx.doi.org/10.1021/nl4041093 | *Nano Lett.* XXXX, XXX, XXX−XXX